Frascati Physics Series Vol. XXX (1997), pp. 000-000
Heavy Quarks at Fixed Target - St. Goar, Oct 3rd, 1996

HEAVY FLAVOUR PRODUCTION IN LEPTON PROTON COLLISIONS AT HERA

Beate Naroska
University of Hamburg
Luruper Chaussee 149
D 22761 Hamburg

ABSTRACT

Recent results on charm production in lepton proton collisions at an e^+p center of mass energy of $\sqrt{s} = 300\,\mathrm{GeV}$ from the experiments H1 and ZEUS are reviewed. Charm is tagged mainly by J/ψ and D^* reconstruction. Results are obtained for "deep inelastic scattering" ($Q^2 > 5 - 10\ \mathrm{GeV}^2$) and in the photoproduction limit ($Q^2 \to 0$). Differential and total cross sections are compared to QCD calculations in next to leading order.

1 Introduction

Charm is produced in positron-proton collisions at HERA almost exclusively in $c\bar{c}$ pairs. The charm quarks are detected either as "open charm", i.e. after hadronization into charmed mesons, such as D^* or D^0. Alternatively "hidden charm" states like J/ψ or ψ' are reconstructed.

The production of charm can occur in *inelastic* collisions, in which colour is transferred from the proton to the charm quark system so that the proton breaks up. On the other hand the vectormesons J/ψ and ψ' can couple directly to the photon and are copiously produced in so–called "diffractive" collisions. These can proceed *elastically* i.e. the proton is conserved or they lead at most to its "dissociation"– break-up of the proton into fragments with low transverse momenta.

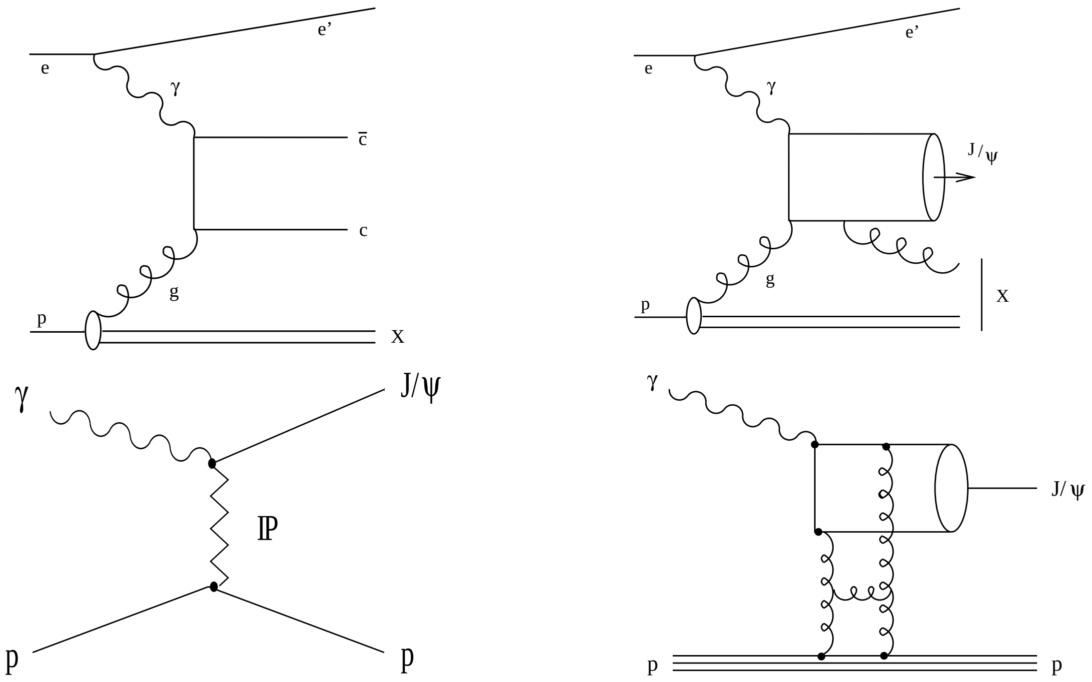

Figure 1: a) Charm production by **photon gluon fusion** and b) formation of a J/ψ in the **Colour Singlet Model**.; c)**Diffractive** J/ψ production; d) same in the **Ryskin** model.

The theoretical description of the *inelastic* production of charm is based on the photon-gluon fusion mechanism, where the positron radiates a photon which participates in the hard interaction with a gluon from the proton to form a $c\bar{c}$ pair (diagram 1a). The hard interaction is calculable in perturbative QCD, and the process is sensitive to the gluon content of the proton. To achieve a colourless J/ψ state at least one further gluon must be involved in the interaction. In the colour-singlet model [1] the radiation of a gluon from a quark line to form a colourless $c\bar{c}$ state is part of the hard interaction (diagram 1b). The colour-octet model [2, 3] has received increased attention lately since it has been proposed to explain the large excess of heavy flavour production rates observed in $p\bar{p}$ collisions [4]. In this model the transition from the coloured $c\bar{c}$ state produced in the hard sub-process proceeds non-perturbatively via emission of soft gluons.

Photon gluon fusion models were extensively tested in fixed target experiments and were found to describe the general features of the data well up to an overall so–called k-factor which was introduced to compensate for missing next-to-leading order (NLO) contributions. Meanwhile NLO calculations have become available for production of open charm [5, 6] and also for J/ψ production in the Colour Singlet Model [7, 8]. Important parameters which determine the size and shape of the cross section are – in addition to the gluon density in the proton – the value of the charm quark mass and the renormalisation scale of QCD.

Charm can also be produced in collisions in which the photon does not participate directly in the hard sub-process but fluctuates into partons. The interaction of these partons with the proton – so called ' resolved' interactions are regarded as a background in the studies reviewed in this paper.

Diffractive production of light vector mesons (ρ, ω, ϕ) has traditionally been described in Regge theory by pomeron exchange [9]. The Vector Dominance Model relates photoproduction of vector mesons to hadron scattering (diagram 1c). This picture has been extended to J/ψ and also ψ' meson production [10]. The important prediction of such models is a cross section proportional to $W_{\gamma p}^{\delta}$, where $W_{\gamma p}$ is the centre-of-mass energy in the γp collision. For this so-called 'soft pomeron' a value $\delta \lesssim 0.32$ is expected. In attempts to understand the nature of the pomeron within QCD it has been conjectured that it is a system of at least two gluons [11]. Ryskin et al have developed a model [12] in which the pomeron is replaced by gluon ladders (diagram 1d) which can be calculated in perturbative QCD in leading logarithmic approximation (LLA). In order to apply the model in photoproduction processes ($Q^2 \to 0$) one has to assume that the charm quark mass offers a hard scale. In this case the cross section is proportional to the square of the gluon density in the proton at Bjorken $x \approx m_{J/\psi}^2/W_{\gamma p}^2$, and a much steeper rise with $W_{\gamma p}$ than in the soft pomeron case is predicted using current measurements of the gluon distribution in the proton.

In summary, the motivation to study charm production at HERA is twofold: it allows a test of perturbative QCD in NLO and a direct determination of the gluon density in the proton. A new understanding of diffractive processes in the framework of QCD and the transition from "soft" to "hard" processes might emerge from the studies of diffractive J/ψ and ψ' production.

2 Kinematics and Gluon Densities

The gluon density in the proton is not very well known. Current parametrisations [14] are shown in fig. 2a. These parametrisations are derived together with the quark densities from data using QCD inspired models. HERA data that contribute are e.g. measurements of the structure function F_2 and its scaling violations. Fig. 2b shows as an example of an F_2 measurement at a scale $Q^2 = 12$ GeV^2 with some of the model "predictions". A strong rise is observed in F_2 towards decreasing x. The assumption is that this rise is driven by the increase of the gluon distribution. Hence only gluon distributions increasing towards low x_g give a good description of the data, e.g. MRSH or GRV, while MRSD0 is too flat to describe the data. For charm production the QCD "scale" μ is the charm quark mass[1] for photoproduction, in electroproduction Q^2 sets the scale.

The kinematic variables used to describe the production of charm pairs will be briefly mentioned here. The reaction and four vectors are:

$$e^+(k) + p(P) \rightarrow e(k') + c\bar{c}(P_c) + X(P')$$

The system $c\bar{c}$ can be replaced by a vectormeson.

- $s = (k+P)^2$, the squared centre of mass energy
- $Q^2 = -q^2 = (k-k')^2$, the squared 4–momentum transferred at the $e\gamma$ vertex
- $t = (P-P')^2$, the squared 4–momentum transferred at the pX vertex
- $W^2_{\gamma p} = W^2 = (q+P)^2 = (P_c + P')^2$, the squared center of mass energy of the γp system
- $x = \frac{Q^2}{2qP}$, the Bjorken scaling variable
- $y = \frac{qP}{kP}$, in the p rest frame y is the fraction of the e's energy carried by the γ
- $z = \frac{P_c \cdot P}{q \cdot P}$, in the p rest frame z is the fraction of the γ's energy carried by the $c\bar{c}$ system.

The highest rate of charm production is expected at low values of Q^2 due to the photon propagator. The experimental results are obtained in two distinct regions of Q^2 due to different experimental procedures: the "photoproduction" limit $Q^2 \rightarrow 0$ is in practice defined by the fact that the scattered positron is not visible in the main detector, which is equivalent to $Q^2 \lesssim 4$ GeV^2. "Electroproduction" on the other hand demands $Q^2 \gtrsim 5-10$ GeV^2 which means that the scattered positron can be measured.

The results presented are based upon data recorded by the H1 [15)] and ZEUS [16)] detectors during 1994 and 1995, when positrons with energy 27.5 GeV and protons of energy 820 GeV were collided in HERA. The integrated luminosities

[1] Photoproduction of D^* uses $\mu = m_c$ or $\mu = \sqrt{m_c^2 + p_t^2}$, production of J/ψ in the Ryskin model $\mu = m_{J/\psi}/2$. Inelastic J/ψ production uses $\mu = m_{J/\psi}$ in leading order and $\mu = \sqrt{2}\, m_c$ in NLO. For finite Q^2 $\mu = \sqrt{Q^2 + 4\, m_c^2}$ is used.

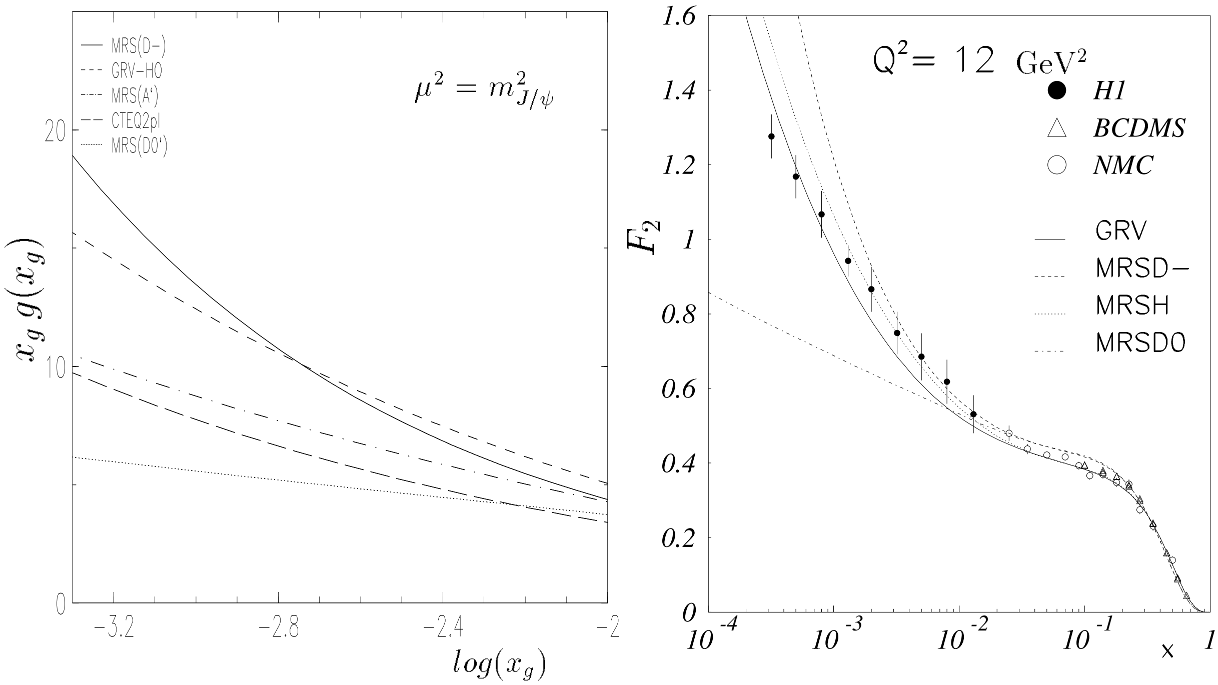

Figure 2: Gluon density parametrisations as a function of x_g, the gluon momentum relative to that of the proton, from various models at a scale of $\mu^2 = m^2_{J/\psi}$ (left); measured F_2 as a function of $x_{Bjorken}$ compared to the prediction by some of these models (right).

delivered by HERA were approximately 1.5 pb^{-1} in 1993, 6 pb^{-1} in 1994 and more than 12 pb^{-1} in 1995. Note however that the integrated luminosities collected by the experiments that can be used for analysis are considerably smaller.

3 Production of "Open" Charm

Tagging of "open charm" events uses well known techniques like reconstruction of the decay[2]:

$$D^{*+} \to D^0\, \pi^+_{slow} \qquad \text{with} \quad D^0 \to K^-\, \pi^+$$

Due to the small mass difference between D^* and D^0 the signal can be seen in the mass difference $\Delta\, M = M(K^-\, \pi^+ \pi^+_{slow}) - M(K^-\, \pi^+)$ as a sharp peak (compare fig. 3). The ZEUS collaboration have also used different decay modes of the D^0, as e.g. $K^-\, \pi^+\, \pi^+\, \pi^-$ and $\overline{K^0}\, \pi^+\, \pi^-$ to reconstruct the D^*. H1 have also reconstructed D^0 directly produced by hadronisation of the c quark (see fig. 3).

3.1 Electroproduction of D^* and D^0

The production of D^* and D^0 in events in which the scattered electron has been identified, and hence $Q^2 \gtrsim 5 - 10\ \mathrm{GeV}^2$ has been studied with the H1 [17)] and ZEUS [18)]

[2]Henceforth charge conjugate states are always assumed to be included although not mentioned.

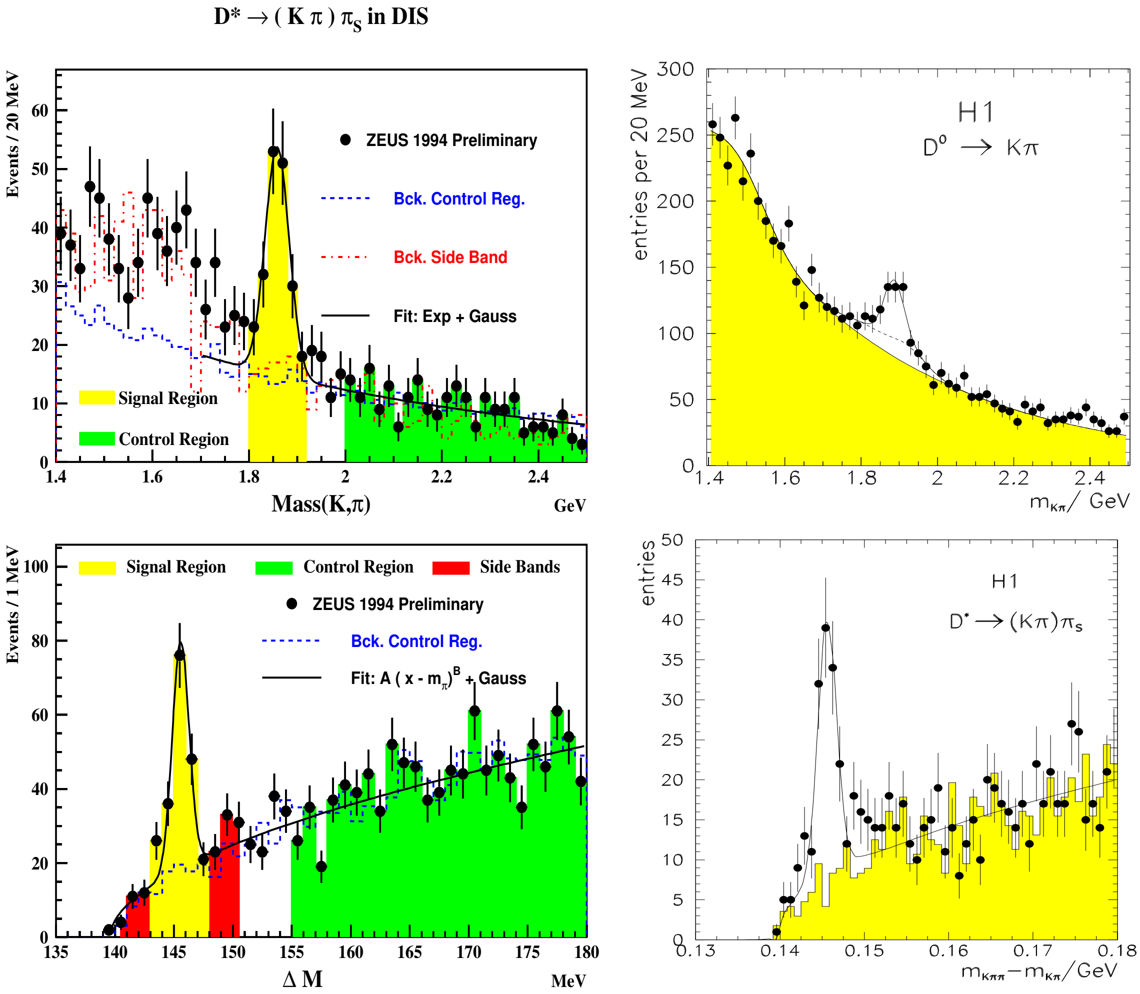

Figure 3: Reconstruction of D^* decays in the ZEUS detector (left): the top figure shows the $K\pi$ mass distribution for $143 < \Delta M < 148$ MeV while the lower figure shows ΔM for the $K\pi$ signal region. Right: D^0(top) and ΔM(bottom) for D^* reconstruction from H1.

detectors. Data can be compared to the Monte Carlo generator AROMA [19] which models photon gluon fusion in leading order for heavy flavour production including mass effects. In fig. 4 data from ZEUS are shown as a function of the γp center of mass energy in the measured kinematical region (see caption of fig. 4). They are compared to a simulation using AROMA with the GRV-LO gluon distribution and three different values for the mass of the charm quark. For comparison a different gluon distribution is also shown. The D^* cross section in this visible kinematical region is $5.4 \pm 1.1 \pm 0.6$ nb.

The p_t distribution obtained by H1 is shown in fig. 5. It is well described by the AROMA simulation. H1 extrapolates from the visible D^0 and D^* cross-sections to the total $c\bar{c}$ cross-sections and obtains $17.4 \pm 1.6 \pm 1.7 \pm 1.4$ nb using the fragmentation fraction $B_{c \to D^*} = 0.260$ [20]. The first error is statistical, the second one systematic and the third error is due to the extrapolation procedure. The ratio

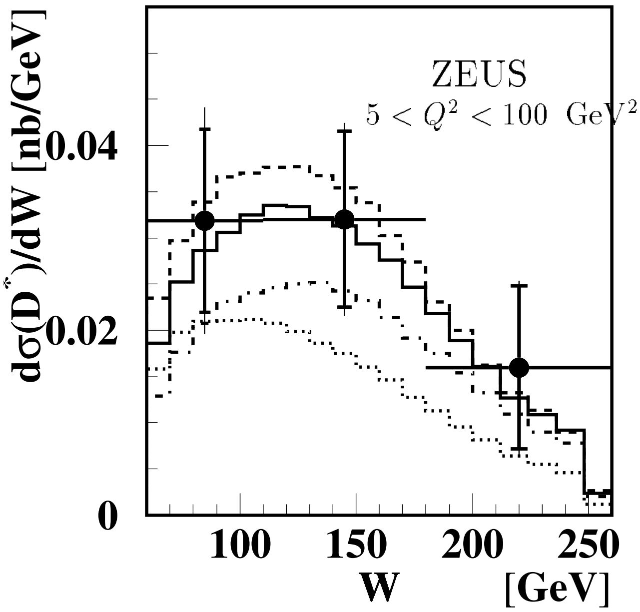

Figure 4: Cross section for $ep \to D^* X$ in the kinematical region: $5 < Q^2 < 100$ GeV$^2, 0.04 < y < 0.7, |\eta| < 1.5$ and $1.3 < p_t < 9.0\,$GeV. The curves indicate photon gluon fusion predictions as calculated by AROMA using the GRV-LO gluon density and $m_c = 1.5$ GeV (full curve), The effect of a variation of m_c by $+0.3$ (dash-dotted) and -0.150 GeV (dashed) is also shown. The dotted curve shows a different gluon density, CTEQ2pL.

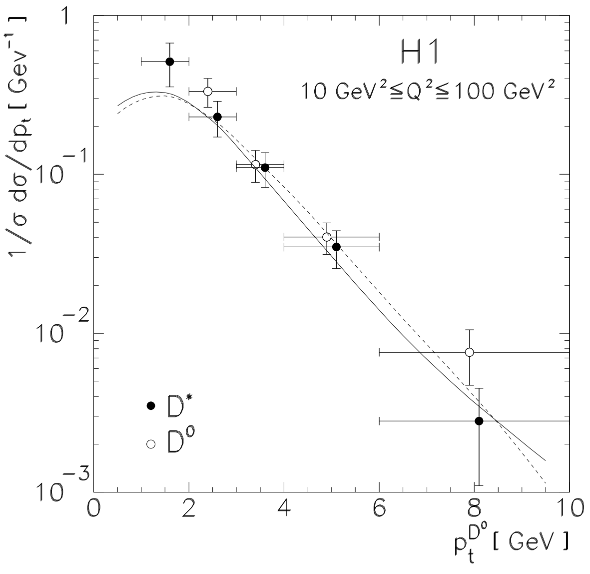

Figure 5: Corrected normalized distributions from the D^{*+} and D^0 analysis: $1/\sigma\, d\sigma/dp_t(D)$ compared with AROMA with $m_c = 1.5\,GeV$ (full curve), and $m_c = 1.3$ GeV (dashed curve, MRSH gluon density, $10 < Q^2 < 100$ GeV^2).

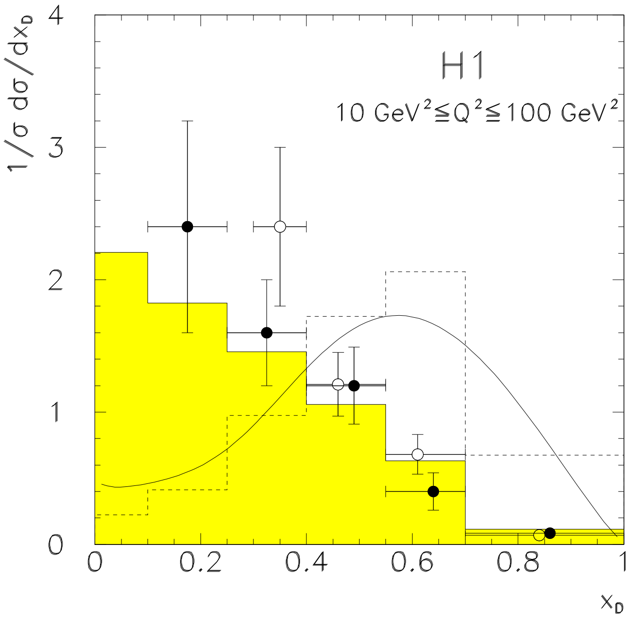

Figure 6: Corrected normalized distributions from the D^{*+} and D^0 analysis: $1/\sigma\, d\sigma/dx_D$ compared with a photon gluon fusion prediction (AROMA) with $m_c = 1.5$ GeV (shaded histogram), a charm sea simulation (LEPTO, dashed histogram), and an expectation from νN scattering evolved to HERA energy. (MRSH gluon density)

of D^* to D^0 production is $0.38 \pm 0.07 \pm 0.06$ which agrees well with measurements in e^+e^- collisions and in hadron hadron interactions (see [17]) for references).

Studying the energy spectrum of the D-meson can shed light on the production process. This analysis is carried out by H1 in the $\gamma^* p$ center of mass system. The normalized distribution of $x_D = \frac{E_D}{W/2}$ is shown in fig. 6 for D^* and D° production. The data obtained by H1 are compared to the predictions of γg fusion as modelled in the AROMA simulation which yields a soft D^* spectrum. A charm "sea" component modelled with the LEPTO/MEPS Monte Carlo generator [21]) yields a harder x_D spectrum than observed in the data. For comparison a measurement of the strange sea component by ν N experiments which does show this hard behaviour is also shown in fig. 6 (evolved to the HERA center of mass energy). Estimating the hard sea contribution in the H1 data leads to an upper limit of 5% at 95% confidence level.

The cross-sections for $c\bar{c}$ production at different values of Q^2 for $0.01 < y < 0.7$ are shown in figure 7 in the form of $F_2^{c\bar{c}}$, the charm contribution to the

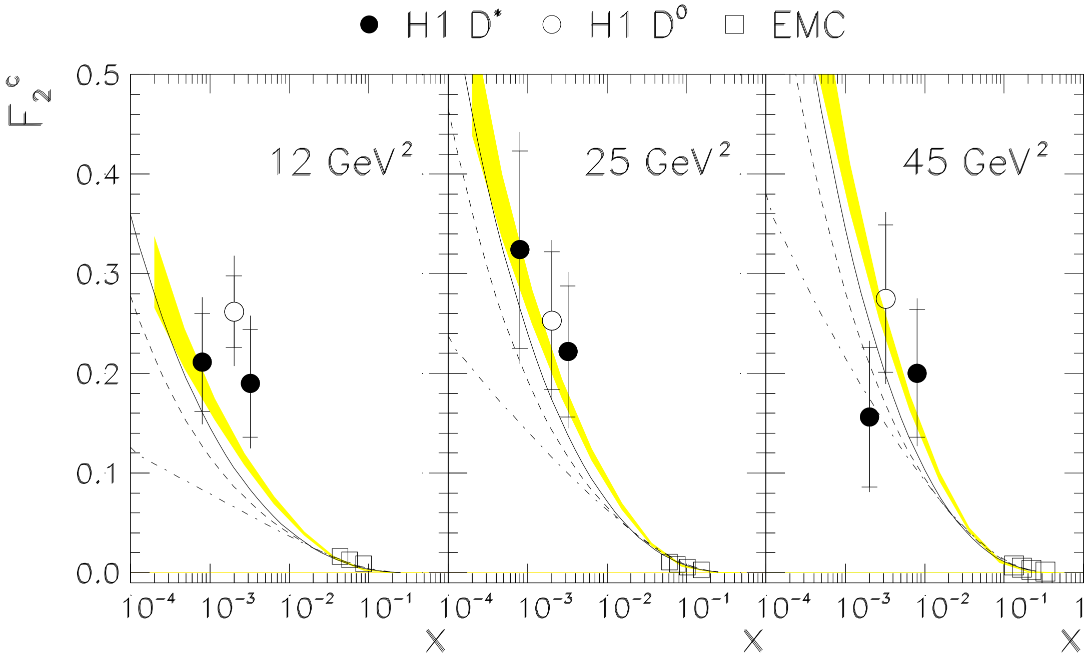

Figure 7: $F_2^{c\bar{c}}$ measurements from H1 D^0 (full circles), H1 D^* (open circles) and EMC (squares) analyses. Inner error bars are statistical, outer total. Compared to NLO calculations based on GRV-HO (full line), MRSH (dashed line), MRSD0' (dash-dotted line), H1 F_2 measurements [22] (shaded stripe).

proton structure function, where

$$\frac{d^2\sigma^{c\bar{c}}}{dx dQ^2} = \frac{2\pi\alpha^2}{Q^4 x}\left(1 + (1-y)^2\right) F_2^{c\bar{c}}\left(x, Q^2\right). \tag{1}$$

A sharp rise of $F_2^{c\bar{c}}$ with decreasing Bjorken x, is observed compared to the fixed target measurements of the EMC collaboration [23] at x–values of $\sim 10^{-1}$. NLO QCD predictions [5] based on various common parametrizations of the proton structure are below the measured values. A calculation based on a fit to the H1 F_2 measurements comes closest to the data. The measured ratio $F_2^{c\bar{c}}/F_2$ is found to be compatible with being constant over the visible kinematic range, with an average value of $0.237 \pm 0.021 \pm^{0.043}_{0.039}$.

3.2 D^* Photo-production

D^* mesons are identified in the H1 and ZEUS detectors by the decay $D^{*+} \rightarrow D^0\pi^+$, in the kinematic region where the transverse momentum of the D^* meson is greater than 2.5 or 3 GeV and its rapidity η between -1.5 and 1.0. Events where the scattered positron is found in the main detector are rejected. The average value of

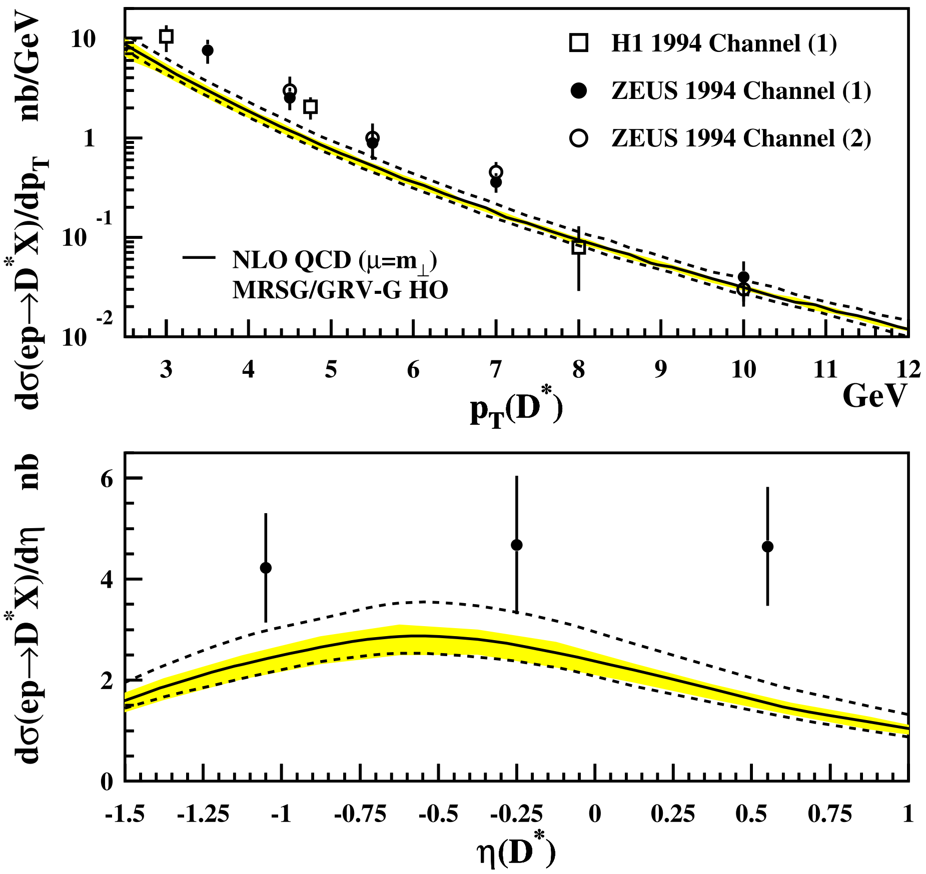

Figure 8: Differential cross sections for $\boldsymbol{ep \to D^* X}$ in the **photoproduction limit** $Q^2 < 4$ GeV^2. Channal (1) denotes the decay $D^* \to (K\pi)\pi_{slow}$ and channel (2) $D^* \to (K\pi\pi\pi)\pi_{slow}$. The curves are predictions by the NLO calculation. a) p_t distribution for data obtained by ZEUS and H1 for $-1.5 < \eta < 1.0$; b) η distribution from ZEUS for $p_t > 3.0$ GeV; the dashed curves in a) and b) show variations by varying the renorm./fact. scale by a factor of 2 or 0.5. The shaded band shows the influence of a variation in m_c.

Q^2 is below 0.05 GeV^2. ep cross sections are converted to γp cross sections assuming factorization and dividing by the photon flux as given by the Weizsäcker-Williams Approximation [24].

A comparison of differential distributions in rapidity and transverse momentum from H1 [25] and ZEUS [26] with the NLO calculations [6] is shown in fig. 8 and 9. The data are above the calculations for the choices of the parameters indicated. In the rapidity distributions even the description of the shape seems to pose problems. In the visible kinematic region described above, the cross-section measurements are found to be insensitive to the parton density parametrizations (fig. 9) and it is not possible to distinguish between them. The total photo-production cross-section $\sigma(\gamma p \to c\bar{c}X)$ is inferred by extrapolating from the restricted kinematic range

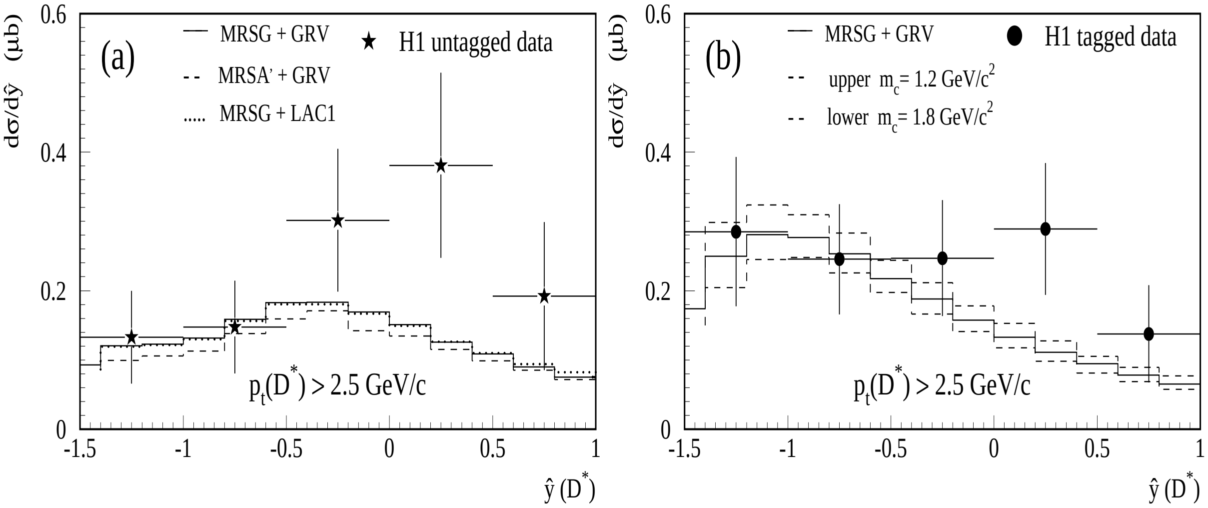

Figure 9: Differential $\boldsymbol{\gamma p}$ **cross sections** $d\sigma/d\hat{y}$ where $\hat{y}$ is the D^* rapidity in the laboratory frame. Data in the **photoproduction limit** $Q^2 < 4$ GeV^2 are compared to NLO predictions. The influence of varying the parton distributions is indicated in a). b) H1 'tagged' refers to a region where the scattered e^+ was detected in the low angle electron tagger, corresponding to $Q^2 < 10^{-2}$.

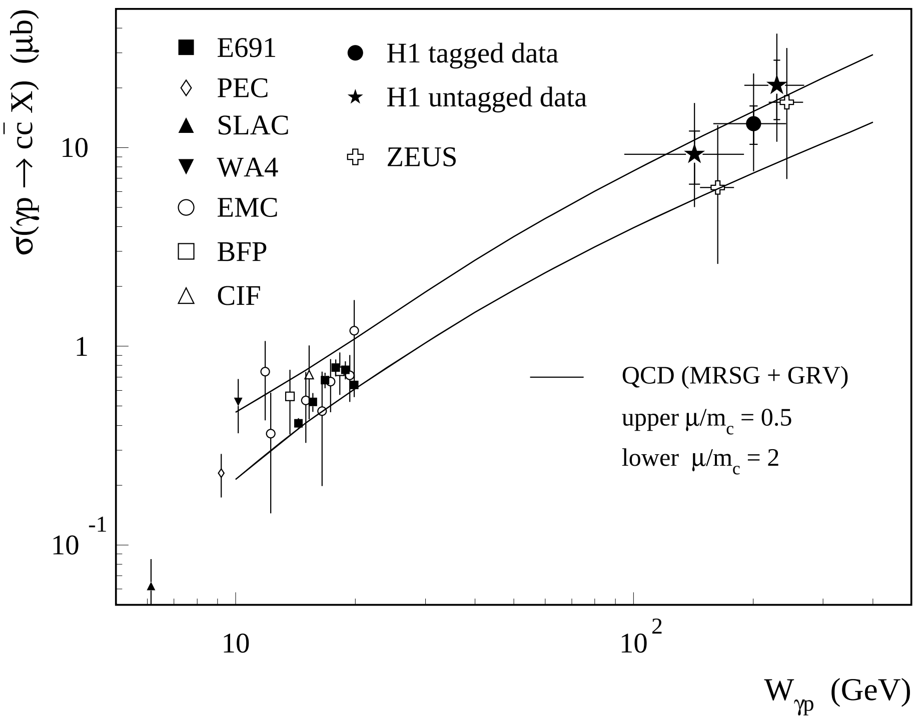

Figure 10: Total **charm photo-production** cross-section as a function of $W_{\gamma p}$, including results from fixed-target experiments , and predictions of NLO QCD calculations with MRSG and GRV-G HO parton density parametrizations. For explanation of H1 'tagged', see fig. 9.

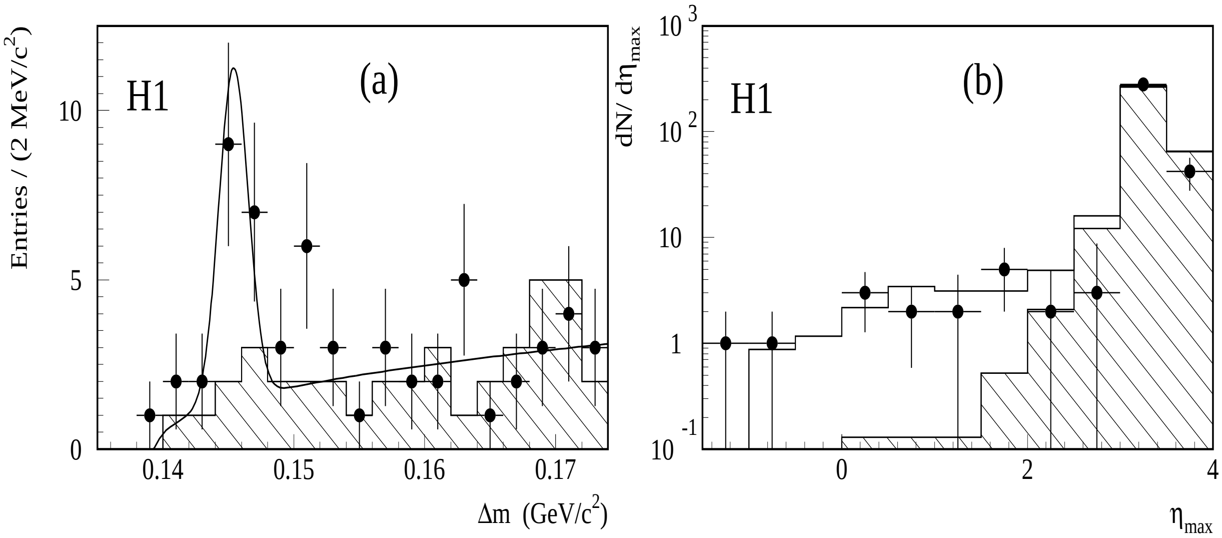

Figure 11: Production of $\boldsymbol{D^*}$ **in events with a large rapidity gap** in photo-production ($Q^2 < 4$ GeV^2). a) $\Delta M = M(K^- \pi^+ \pi^+_{slow}) - M(K^- \pi^+)$ for $\eta_{max} < 2$. b) η_{max} distribution of D^* candidate events. The hatched histogram shows a non-diffractive model (Pythia [27]), the solid histogram the sum of the non-diffractive model and a diffractive one (RAPGAP [28]).

to the total cross-section for D^* production. The result is shown in figure 10 where the inner error bars represent the combined statistical and systematic errors, and the outer error bars include the large uncertainty in the extrapolation which arises due to the possible choices of parton density parametrizations outside the measured kinematical regions. The prediction of a NLO QCD calculation [6] is shown for two extreme values of the renormalization scale as indicated.

A strong rise of the photo-production cross-section of charm with $W_{\gamma p}$, with respect to earlier results from lower energy collisions, is observed.

3.3 Diffractive D^* production

In the study of ep scattering at HERA events were found by the ZEUS and H1 collborations [29] which have a large gap in the energy flow in the rapidity region close to the direction of the scattered proton. The nature of these events can be understood if a diffractive mechanism is invoked where no colour is exchanged between the observed hadronic system and the proton remnant [30]. The rate of these events is roughly 10% of the "normal" ones – where such a gap in the energy flow does not exist – and many models have been put forward to explain them.

In view of understanding the production mechanism an interesting question to be asked is whether charm is produced in events with a large rapidity gap. H1 has looked for D^* events with a large rapidity gap in photoproduction [25] and also at high Q^2 [31]. The signals are shown in fig. 11a for photo production events in which

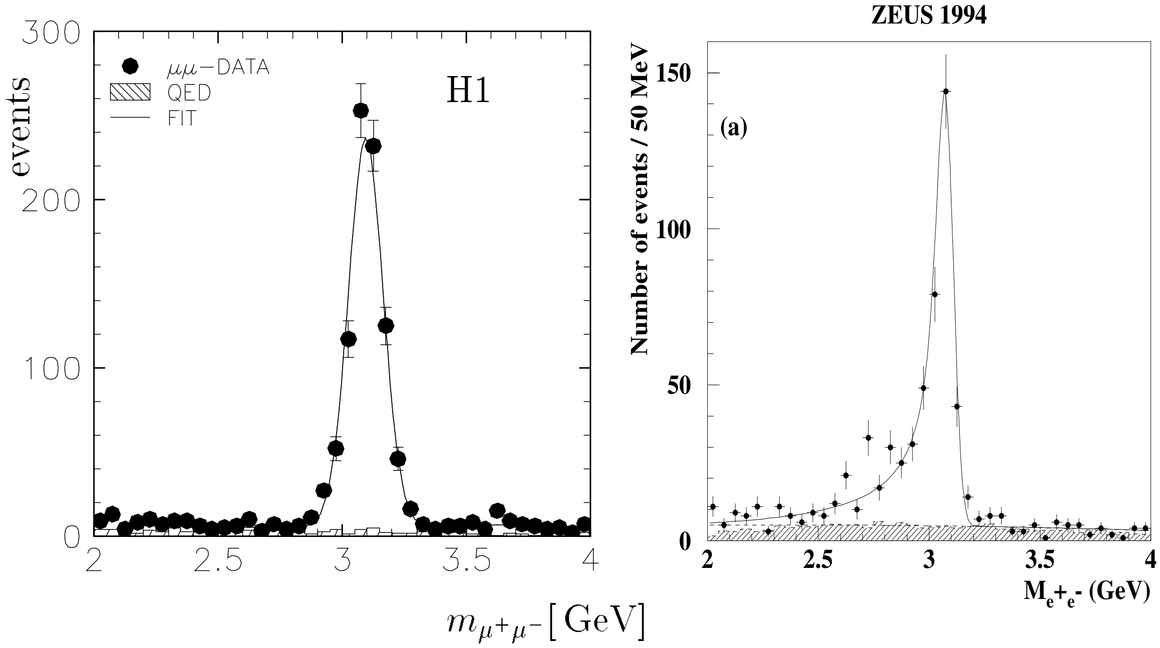

Figure 12: Mass distribution for $\mu^+\mu^-$ pairs (H1) and e^+e^- pairs (ZEUS) in the J/ψ mass region for diffractive J/ψ production.

the energy deposit with largest rapidity is registered at values of $\eta_{max} < 2$. The distribution of η_{max} is shown in fig. 11b. The data in fig. 11b cannot be explained by a standard QCD based simulation but are well described if a diffractive component is added. Although errors are large the rate of events seen is more consistent with a gluon dominated diffractive exchange than with a quark dominated exchange. Studying events with a large rapidity gap in data at large Q^2 leads to a similar conclusion: a diffractive component is required and a gluon dominated exchange is preferred.

4 Production of J/ψ and ψ' Mesons

Here we will discuss photoproduction of J/ψ and ψ', where most of the data have been accumulated. First signals of J/ψ meson production at high Q^2 ($Q^2 \gtrsim 10$ GeV^2) have also been analysed [33].

4.1 Inelastic Photo-production of J/ψ Mesons

J/ψ mesons are identified by their decays to muon or electron pairs, see fig. 12. In order to select *inelastic* events additional activity is required in the detector and the data are restricted to $z < 0.9$ to exclude diffractive contributions. (see section 2 for

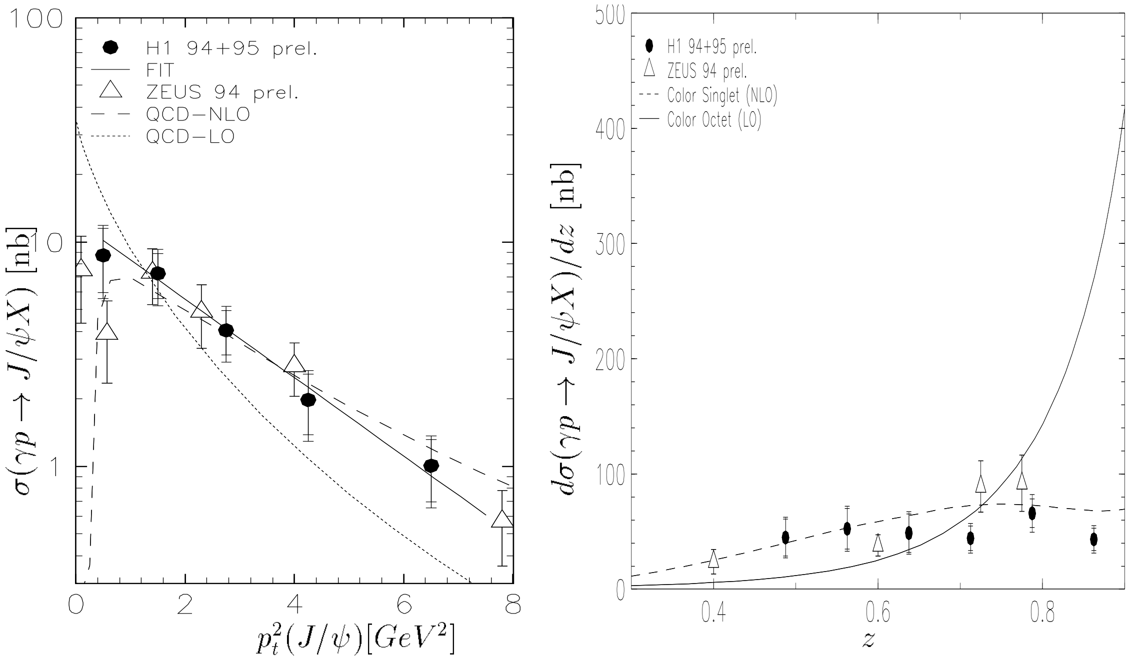

Figure 13: **Inelastic photo-production of J/ψ.** a) p_t^2 distribution compared to NLO and LO QCD calculations in the colour-singlet model. b) Differential photo-production cross-section for J/ψ in the variable z, compared to predictions of the colour-singlet (NLO) and colour-octet (LO) models.

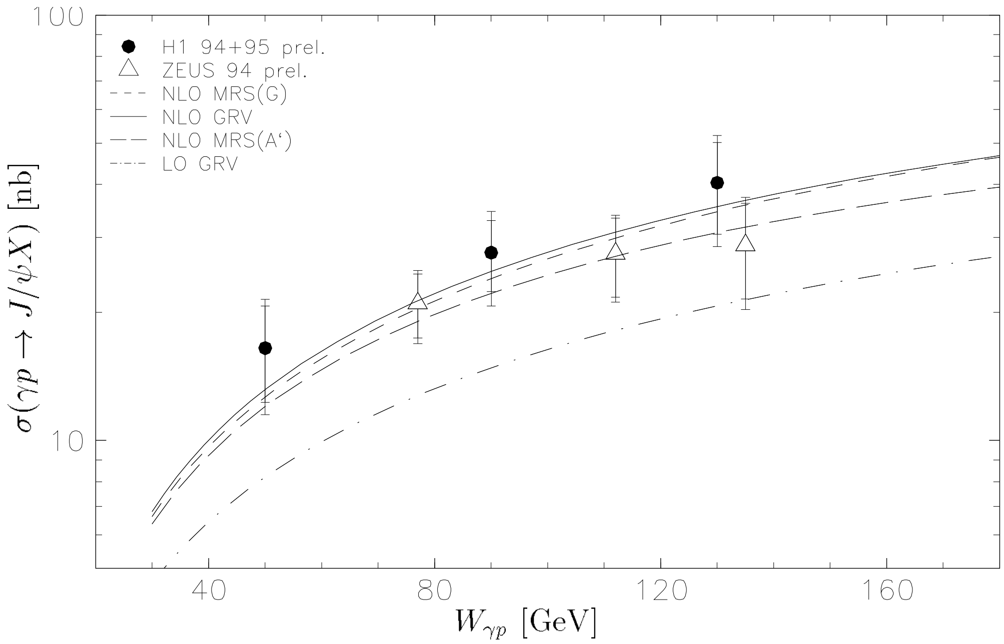

Figure 14: Cross-sections for **inelastic photo-production J/ψ mesons** in the limits $z < 0.8$, $p_t > 1$ GeV^2, compared to NLO and LO QCD calculations in the colour-singlet model based on the parton density parametrizations MRSG , GRV-LO, MRSA'. Inner error bars statistical, outer total.

the definition of z). A lower cut in z rejects events from resolved photon events. The final cross section values are corrected for the loss due to the lower z-cut ($\approx 20\%$).

The distribution of p_t^2 for inelastic J/ψ events is shown in fig. 13 for data from H1 [32] and ZEUS [34] for $z < 0.8$. The data are well described by the prediction of the NLO QCD calculations in the Colour Singlet Model except at low values of p_t^2, where contributions of higher order (next-to-next-to leading order) can become substantial. The leading order calculation which is also shown, is much steeper than the data.

The total γp cross section for $p_t(J/\psi) > 1\,\mathrm{GeV}$ and $z < 0.8$ is shown as a function of the γp center of mass energy in fig. 14. The prediction of the NLO QCD calculations fit the data well in shape and in absolute normalisation. The parameters used are: charm quark mass $m_c = 1.4$ GeV renormalisation/factorisation scale $\mu = \sqrt{2}m_c \sim 2$ GeV and $\Lambda_{QCD} = 0.300$ GeV. The theoretical curves also contain a correction for the contribution from cascade decays of ψ', which are not separated experimentally. As can be seen in fig. 14 the dependence of the cross section on the gluon density parameterisation is not strong with the given cuts. All gluon parametrisations which fit recent F_2 data at low x, such as GRV or MRSG or MRSA' give a good description of the data within errors.

As can be seen in figure 13, the differential cross-section in z is also well reproduced by the calculation based on the colour-singlet model, but contains no indication of the sharp rise towards high z which is predicted in the colour-octet model in leading order if the long range matrix elements are chosen from fits to the CDF data [3].

4.2 Diffractive Production of J/ψ

Cross-sections for the *elastic* interaction $\gamma p \to J/\psi p$ are measured by isolating a sample of events where no energy deposit is found in the detector other than that associated with the decay products of the J/ψ meson. The remaining inelastic contamination is subtracted statistically. A strong rise of the cross-section with increasing $W_{\gamma p}$ is observed (figure 16), which is significantly beyond that expected for interactions mediated by a soft pomeron ($\delta \lesssim 0.32$). Rather, a value $\delta = 0.60$ provides a better fit to the H1 and ZEUS measurements. Including the fixed target data yields $\delta \approx 0.9$ in this simple description.

A good description of the rise in the cross-section is obtained by calculations in the Ryskin model [12, 13] using a scale of $m_\psi^2/4$. In figure 16, curves are shown for two common parametrizations of the proton structure. The absolute

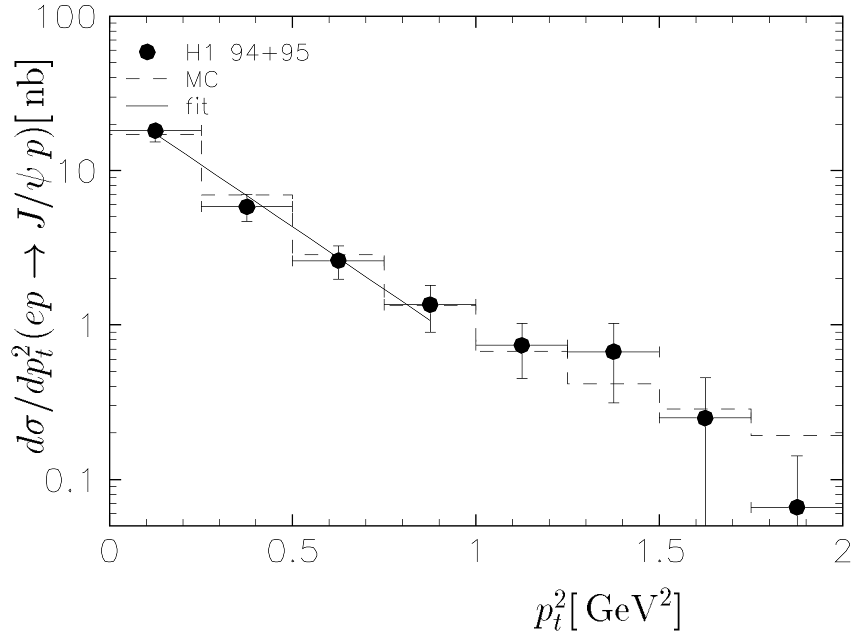

Figure 15: **Elastic J/ψ-Production:** Differential cross section $d\sigma/dp_t^2(ep \to J/\psi\, p)$ with a fit to the form $\exp(-bp_t^2)$ and a Monte-Carlo-prediction (DIF-FVM [36]).

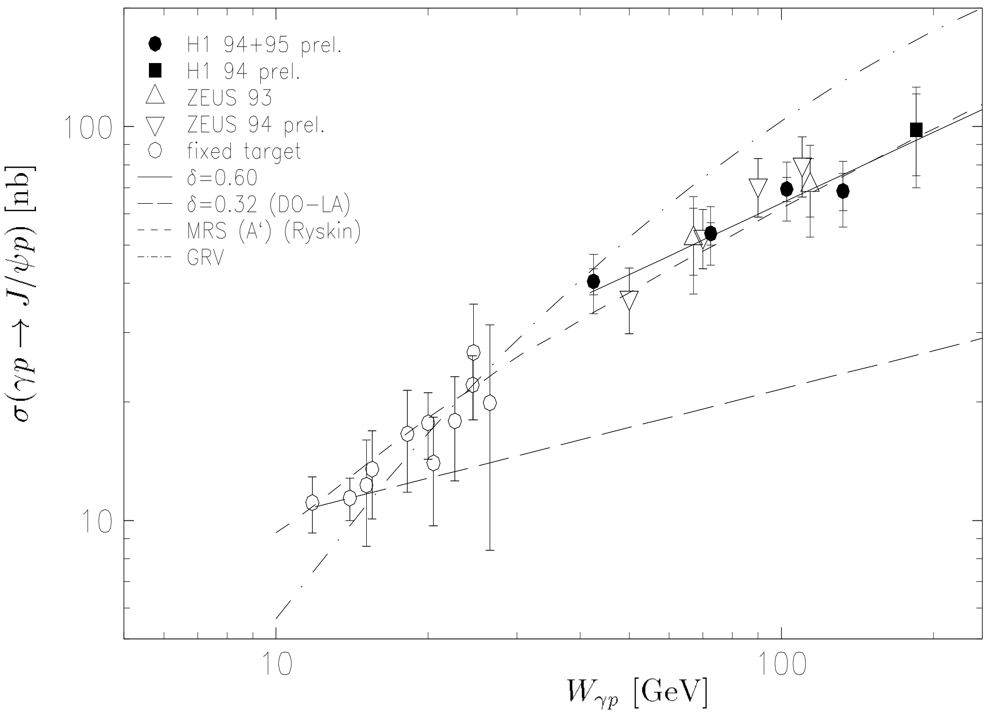

Figure 16: **Elastic photo-production cross-section for J/ψ** vs $W_{\gamma p}$. Inner error bars statistical, outer total. Parametrizations of the $W_{\gamma p}$ dependence as $W_{\gamma p}^{0.6}$ and $W_{\gamma p}^{0.32}$, and calculations according to the Ryskin modelfor gluon density functions as shown. Included are results from fixed target experiments [37].

normalization of the calculations is only reliable to approximately 30%, so that only the shapes should be used to distinguish between different parametrizations.

Apart from the steep rise of the elastic cross section with γp center of mass energy the data agree with the standard diffractive expectations: the t-distribution is exponential, see fig. 15 where t has been approximated by p_t^2. The b slope for the elastic interaction $ep \to J/\psi p$ is measured using a fit of the form $d\sigma/dp_t^2 \propto e^{-bp_t^2}$ to the data with $p_t^2 < 1$ GeV^2. Values $b = 4.1 \pm 0.2 \pm 0.2$ GeV^{-2} for $30 < W_{\gamma p} < 150$ GeV are obtained by H1 and $b = 4.0 \pm 0.4 \pm 0.5$ GeV^{-2} by ZEUS. The decay angle distributions in the helicity frame are found to agree with helicity conservation by ZEUS.

4.3 ψ' Photo-production

Clear signals for ψ' are seen by searching for the decay to $J/\psi\,\pi^+\pi^-$ in the H1 detector [35] where the J/ψ subsequently decays to a lepton pair, and insisting that no further charged particles are identified (figure 17). The acceptance is limited to the kinematic region $z > 0.95$, where a ratio for the photo-production cross-sections, $\sigma(\psi')/\sigma(J/\psi) = 0.16 \pm 0.06$ at $W_{\gamma p} = 80$ GeV is measured. A similar ratio has been found at $W_{\gamma p} < 20$ GeV at other experiments [38].

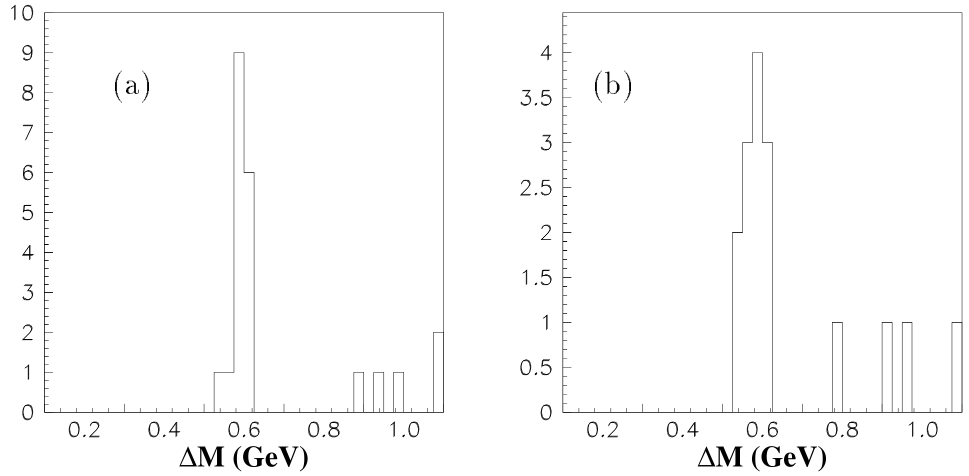

Figure 17: (a) Distribution of $\Delta M \equiv M_{\mu^+\mu^-\pi^+\pi^-} - M_{\mu^+\mu^-}$ for four-prong events where a muon pair is found satisfying $2.8 < M_{\mu^+\mu^-} < 3.4$ GeV. (b) Same for decay $J/\psi \to e^+e^-$.

5 Conclusions

The production of charm quarks in e^+p collisions at HERA has been studied by identifying charm in the form of D^*, D^0, J/ψ and ψ' mesons. Measurements were

performed at $5 < Q^2 < 100$ GeV^2 and in the photoproduction limit.
Inelastic charm production can be described reasonably well by photon gluon fusion models and NLO contributions are found to be important. There is a tendency of the data to be above the calculations for most parametrisations of the gluon density and a value of the charm quark mass of 1.5 GeV.
In *deep inelastic processes*($Q^2 \gtrsim 10$ GeV^2) charm contributes to F_2 at almost 25%. The absolute value of $F_2^{c\bar{c}}$ at x values of typically 10^{-3} is found almost an order of magnitude larger than the EMC measurement at $x \sim 10^{-2}$.
All *photo-production* cross-sections, in particular for $c\bar{c}$ and for inelastic and diffractive production of J/ψ, are found to rise steeply with increasing $W_{\gamma p}$. This characteristic is well described by models based on NLO perturbative QCD in which the rise reflects the increase in the gluon content of the proton towards low x.
The *energy distribution of inelastically produced J/ψ* mesons is well described by the *Colour Singlet Model* in NLO. No indication of large colour octet contributions is seen within statistics.
The *diffractive production of J/ψ* and ψ' increases much faster with $W_{\gamma p}$ than expected in "soft" models with pomeron exchange a la Donnachie and Landshoff. A QCD based model relating the cross section to double gluon exchange successfully describes the data with current parametrizations of the gluon density. Apart from the strong dependence on the center of mass energy the data show an exponential behaviour as a function of t and they agree with s-channel helicity conservation.

Acknowledgments

It is a pleasure to thank the organisers of the workshop for a stimulating and pleasant three days in magnificent surroundings. I thank all H1 and ZEUS members who provided figures and explanations.

References

1. L. Berger, D. Jones, Phys. Rev D23 (1981) 1521
   R. Baier and R. Rückl, Nucl. Phys. B201 (1982) 1
2. G.T. Bodwin, E. Braaten, G.P. Lepage, Phys.Rev. D51 (1995) 1125
3. M. Cacciari and M. Krämer, Phys. Rev. Lett. 76 (1996) 4128
4. F. Abe et al. (CDF Coll.) , Phys. Rev. Lett. 69 (1992) 3704; A. Sansoni, Fermilab-Conf 95/263-E

5. E. Laenen et al., Nucl. Phys. B392 (1993) 162, 229; E. Laenen et al., Phys. Lett. B291 (1992) 325; S. Riemersma, J. Smith, and W.L. van Neerven, Phys. Lett. B347 (1995) 143

6. S.Frixione et al., Phys.Lett. B348, 633 (1995); Nucl.Phys. B454, 3 (1995)

7. M. Krämer, J. Zunft, J. Steegborn, P.M. Zerwas, Phys.Lett. B348 (1995) 657

8. M. Krämer, Nucl. Phys. B459 (1996) 3

9. J.J.Sakurai, Ann.Phys.(NY) 11, 1 (1960); M.Gell-Mann,F.Zachariasen, Phys.Rev. 124, 953 (1961); T.H.Bauer et al, Rev.Mod.Phys. 50, 261 (1978); S.D.Holmes et al., Ann.Rev.Nucl. Part.Sci. 35, 397 (1985)

10. A. Donnachie and P.V. Landshoff, Phys. Lett. B348 (1995) 213 ; ibid. B296 (1992) 227 .

11. P.V. Landshoff, O. Nachtmann, Z.Phys.C 35 (1987) 409

12. M.G.Ryskin, Z.Phys. C57, 89 (1993)

13. M.G.Ryskin et al.,DTP-95-96 (1995),revised Feb 1996

14. A.D.Martin et al., RAL-94-055 (1994) (MRS G); M.Glück et al., Phys.Rev. D45, 3986 (1992)(GRV-G HO); M.Glück et al., Z.Phys. C53 (1992) 127 (GRV-HO); A.D.Martin et al., Phys.Rev.D50 (1994) 6743 (MRSH); A.D.Martin et al., Phys.Lett. B306 (1993) 145 (MRS D0'); M.Glück et al., Phys.Rev. D46 (1992) 1973 (GRV-LO); A.D.Martin et al., Phys.Lett. B354 (1995) 155 (MRS A'); CTEQ Collaboration, as given in the PDFLIB, H. Plothow-Besch/CERN-PPE (CTEQ2pL)

15. H1 Collab., DESY 96-001 (1996)

16. ZEUS Collab., DESY 95-193 (1995)

17. H1 Collab., DESY 96-138 (1996)

18. ZEUS Collab., contribution pa02-031 ICHEP, Warsaw, 1996 [3]

19. G. Ingelman, J. Rathsman, and G.A. Schuler, DESY preprint, DESY 96-058, and HEP-PH/9605285

20. OPAL Collab., CERN-PPE-94/217 (1994)
LEP Collab., CERN-PPE-96/017 (1996)

21. G. Ingelman, "LEPTO version 6.1– The Lund Monte Carlo Generator for Deep Inelastic Lepton-Nucleon Scattering", TSL/ISV-92-0065

22. H1 Collab., Nucl.Phys. B470, 3 (1996)

23. EMC Collab., Z.Phys. C35, 1 (1987); Nucl.Phys. B213, 31 (1983)

[3] "ICHEP, Warsaw, 1996" is used as abbreviation for: XXVIII International Conference on High Energy Physics, 25-31 July 1996, Warsaw, Poland.

24. C.F.Weizsäcker, Z.Phys. 88, 612 (1934)
E.J.Williams, Phys.Rev. 45, 729 (1934)

25. H1 Collab., S. Aid et al., Nucl Phys. B 472 (1996) 32; contribution pa02-088 ICHEP, Warsaw, 1996

26. ZEUS Collab., contribution pa05-051 ICHEP, Warsaw, 1996

27. T. Sjöstrand, CERN-TH-6488(1992), Comp. Phys. Comm. 82 (1994) 74

28. H. Jung, Comp. Phys. Comm. 86 (1995) 147

29. ZEUS Coll., M. Derrick et al., Phys. Lett. B315 (1993) 481; Phys. Lett. B 332 (1994) 228; H1 Collab., T. Ahmed et al., Nucl.Phys. B435 (1995) 3

30. for a review see e.g. J. Dainton, DESY 95-228, 1995

31. H1 Collab., contribution pa02-060 ICHEP, Warsaw, 1996

32. H1 Collab., S. Aid et al., Nucl Phys. B 472 (1996) 3; contribution pa02-085 ICHEP, Warsaw,1996

33. ZEUS Collab., contribution pa02-028 ICHEP, Warsaw,1996; H1 Collab., S. Aid et al., Nucl Phys. B 468 (1996) 3

34. ZEUS Collab., contribution pa02-047 ICHEP, Warsaw,1996

35. H1 Collab., contribution pa02-086 ICHEP, Warsaw, 1996

36. B. List, Diploma Thesis Techn. Univerity Berlin (1993) unpublished

37. E687 Collab., Phys.Lett. B316, 197 (1993);
E401 Collab., Phys.Rev.Lett. 48, 73 (1982);
FTPS Collab., Phys.Rev.Lett. 52, 795 (1984)

38. EMC Collab., Nucl.Phys. B213, 1 (1983);
NA-14 Collab., Z.Phys. C33, 505 (1987);
E401 Collab., Phys.Rev.Lett. 50, 302 (1983)